

Resolved Sideband Cooling of a Micromechanical Oscillator

A. Schliesser, R. Rivière, G. Anetsberger, O. Arcizet, T. J. Kippenberg*
Max Planck Institut für Quantenoptik, 85748 Garching, Germany

Micro- and nanoscale opto-mechanical systems—based on cantilevers [1, 2], micro-cavities [3, 4] or macroscopic mirrors [5, 6]—provide radiation pressure coupling [7] of optical and mechanical degree of freedom and are actively pursued for their ability to explore quantum mechanical phenomena of macroscopic objects [8, 9]. Many of these investigations require preparation of the mechanical system in or close to its quantum ground state. In the past decades, remarkable progress in ground state cooling has been achieved for trapped ions [10, 11] and atoms confined in optical lattices [12, 13], enabling the preparation of non-classical states of motion [14] and Schrödinger cat states [15]. Imperative to this progress has been the technique of *resolved sideband cooling* [16, 17, 18], which allows overcoming the inherent temperature limit of Doppler cooling [19] and necessitates a harmonic trapping frequency which exceeds the atomic species' transition rate. The recent advent of cavity back-action cooling [20] of mechanical oscillators by radiation pressure has followed a similar path with Doppler-type cooling being demonstrated [1, 2, 4, 5, 21], but lacking inherently the ability to attain ground state cooling as recently predicted [22, 23]. Here we demonstrate for the first time resolved sideband cooling of a mechanical oscillator. By pumping the first lower sideband of an optical microcavity [24], whose decay rate is more than twenty times smaller than the eigen-frequency of the associated mechanical oscillator, cooling rates above 1.5 MHz are attained, exceeding the achievable rates in atomic species [10]. Direct spectroscopy of the motional sidebands reveals 40-fold suppression of motional increasing processes, which could enable attaining final phonon occupancies well below unity (< 0.03). Elemental demonstration of resolved sideband cooling as reported here, should find widespread use in opto-mechanical cooling experiments and represents a key step to attain ground state cooling of macroscopic mechanical oscillators [8]. Equally important, this regime allows realization of motion measurement with an accuracy exceeding the standard quantum limit by two mode pumping [25] and could thereby allow preparation of non-classical states of motion.

In atomic laser cooling, the lowest temperature which can be attained for a trapped ion (or atom) whose harmonic trapping frequency Ω_m is smaller than its decay rate γ is given by $T_D \cong \hbar\gamma/4k_B$, the *Doppler limit* [19]. In this "weak binding" regime [19] (cf. Fig 1a), the minimum average occupation number in the harmonic trapping potential is $n_{\min} \approx \gamma/4\Omega_m \gg 1$, which implies that the atoms' harmonic motion cannot be cooled to the quantum ground state. On the other hand, much lower occupation can be attained in the *resolved sideband limit*. Resolved sideband cooling [16, 17] is possible when a harmonically bound dipole such as an atom or ion exhibits a trapping frequency $\Omega_m \gg \gamma$, thereby satisfying the so called "strong binding condition" [19]. The physics behind resolved sideband cooling can be understood as follows. Owing to its harmonic motion, a spatially oscillating excited atom will emit phase modulated radiation $E(t) = E \cos(\omega t + \beta \cos(\Omega_m t))$ with a modulation depth given by $\beta = k \cdot x$, where $k = 2\pi/\lambda$, λ is the wavelength in vacuum and x the displacement amplitude along the emission direction. Consequently the emission spectrum consists of symmetric sidebands of frequencies $\omega_0 - j\Omega_m$ (where $j = \pm 1, \pm 2, \dots$), whose intensities are weighted by Bessel functions $|J_j(\beta)|^2$. Inversely, the absorption spectrum as probed by an observer in the laboratory frame will consist of a series of absorption lines, broadened due to the finite upper state lifetime. Cooling can be achieved by tuning the incident radiation to one of the energetically lower lying sidebands

($\omega_L = \omega_0 - j\Omega_m$, $j = 1, 2, \dots$, cf. Fig. 1a). This entails that the atom absorbs photons of energy $\hbar\omega_L$ while it emits on average energy $\hbar\omega_0$, thereby reducing the ion's or atom's translational energy, leading to cooling. The lowest average occupancy that can be attained is given by [18] $n_{\min} \approx \gamma^2/16\Omega_m^2 \ll 1$, implying that the particle can be found in the ground state most of the time, in contrast to the "weak binding" case. This powerful cooling technique, first proposed by Dehmelt and Wineland [17] in 1975, has been called "cooling by motional sideband excitation" [16] or "sideband cooling" and has lead directly to the remarkable demonstration of ground state cooling of trapped ions [10, 11] and later of atoms in optical lattices [12, 13]. Several interesting extensions of this method exist [26], including proposed techniques in which the ion (or atom) is coupled to a mechanical system [27, 28].

Turning to the opto-mechanical setting consisting of a cavity (optical degree of freedom, with a decay rate κ) with a movable boundary (mechanical degree of freedom, with frequency Ω_m) analogous reasoning can be made. If the strong binding condition is satisfied, i.e. $\Omega_m \gg \kappa$, the cavity will also exhibit—owing to its harmonic motion—an absorption spectrum which possesses both a carrier at the cavity resonance frequency and a series of sidebands at $\omega_0 + j\Omega_m$. Their absorption strength is again proportional to $|J_j(\beta)|^2$, where in the opto-mechanical case of a whispering gallery mode cavity the modulation index is given by $\beta = \omega_0 x/\Omega_m R$,

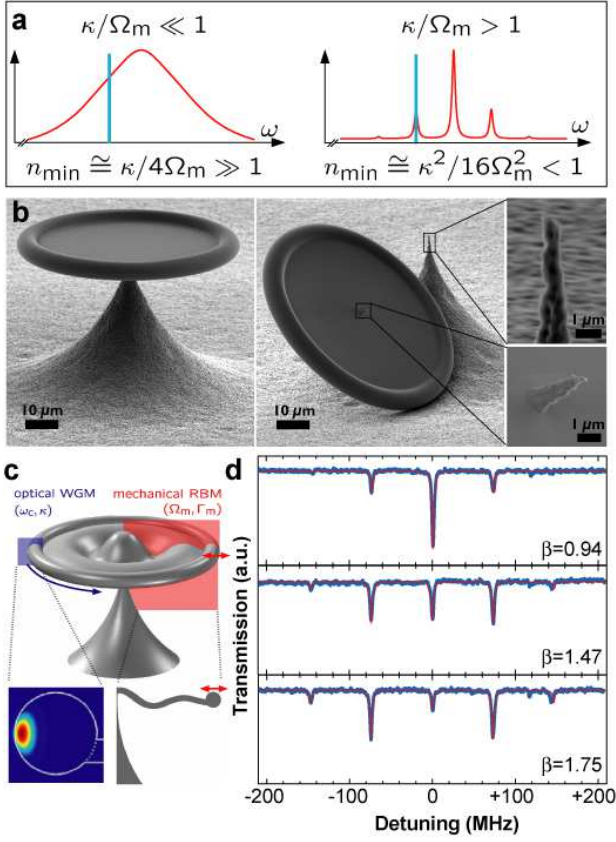


FIG. 1: Resolved sideband regime of an opto-mechanical system. **a** Comparison of the “weak binding” regime, where the mechanical oscillator frequency Ω_m is smaller than the cavity decay rate κ , and the “strong binding” regime with $\Omega_m \gg \kappa$. The minimum achievable average phonon occupancy of the mechanical oscillator is denoted by n_{\min} . Note that only in the limit of well resolved sidebands, ground state cooling ($n_{\min} \ll 1$) is possible. **b** Scanning electron micrograph of the opto-mechanical system used in the present study, consisting of an ultra-high finesse toroidal optical micro-cavity with high- Q radial breathing modes ($Q = 30,000$) supported by a “needle” pillar. Also shown is an image of an *intentionally* broken cavity structure, revealing the ultra thin silicon support pillar with a diameter of 500 nm, which reduces the coupling to the pillar and thus enables high mechanical Q factors. **c** Schematic of the radiation pressure coupling of optical and mechanical mode in the toroidal microcavity. **d** Cavity transmission spectrum of a microtoroid with a mechanical degree of freedom driven with a coherent drive (via radiation pressure back-action amplification [3] using an auxiliary laser beam, cf. SI) for different driving amplitudes. The optical cavity decay rate corresponds to $\kappa/2\pi = 3.2$ MHz while the mechanical breathing mode exhibits a frequency of $\Omega_m/2\pi = 73.5$ MHz, thereby placing the system deeply into the resolved sideband regime. The weights of the sidebands follow the Bessel function expansion (solid line is a fit).

where R denotes the cavity radius and x the mechanical oscillation amplitude. This factor can be rewritten as $\beta = kx2\pi/\Omega_m\tau_{\text{rt}}$, implying that compared to the atomic dipole case the coupling is enhanced by the number of

cavity round trips (of time τ_{rt}) the photon completes during one mechanical oscillation period. Laser cooling can be achieved by tuning the incident radiation to the first lower sideband. Thus the optical cavity resonance now plays the role of the ion’s optical transition in the frequency up-conversion process [23]. Recent theoretical work has demonstrated [22, 23] that, analogous to the ion trapping case [19], final occupancies in the mechanical degree of freedom below unity can exclusively be attained in the resolved sideband regime. In brief and as shown in Refs [22, 23], the quantum mechanical cooling limit is due to the fact that cooling proceeds both by motional increasing and decreasing processes. Motional decreasing (increasing) processes constitute absorption on the lower (upper) sideband and emission on the carrier and occur with a rate $R^{\text{LSB}} \propto \eta^2 A^- n$ ($R^{\text{USB}} \propto \eta^2 A^+ (n+1)$), where n is the phonon occupancy, $A^\pm \propto ((\kappa/2)^2 + (\Delta \mp \Omega_m)^2)^{-1}$ and η an effective parameter [23] $\eta = \omega_0 x_0 / \Omega_m R$ with $x_0 = \sqrt{\hbar/m_{\text{eff}}\Omega_m}$ being the zero point motion of the mechanical oscillator mode. Detailed balance [29] then yields the minimum average occupancy $n_{\min} = A^- / (A^- - A^+)$ neglecting reservoir heating. In the “weak binding” limit $\Omega_m \ll \kappa$ this prevents ground-state cooling as $n_{\min} \approx \kappa/4\Omega_m \gg 1$, recovering the Doppler limit. On the other hand, occupancies well below unity can be attained in the resolved sideband case $\Omega_m \gg \kappa$ yielding $n_{\min} \approx \kappa^2/16\Omega_m^2 \ll 1$. Tuning a laser with power P to the first lower sideband ($\Delta = -\Omega_m$), the cooling rate $\Gamma_c = A^- - A^+$ under these conditions is given by [4]:

$$\Gamma_c \approx \frac{8\omega_0}{\Omega_m} n^2 F^2 \frac{P}{m_{\text{eff}} c^2} \frac{\tau}{\tau_{\text{ex}}} \frac{1}{1 + 4\tau^2 \Omega_m^2}. \quad (1)$$

Here F denotes the cavity finesse, n the refractive index of the cavity material, m_{eff} the effective mass of the mechanical mode, c the speed of light *in vacuo*, $\tau = \kappa^{-1}$ the total photon lifetime and τ_{ex} denotes the lifetimes only due to output coupling. Note that when working in this regime of a highly detuned laser, the mechanical frequency shift, or optical spring, is negligible, and the radiation pressure force is mainly viscous. While several groups have recently reported radiation pressure cooling of a mechanical oscillator [1, 2, 4, 5], these experiments have all fallen into the regime of “weak binding”, owing to the challenge of simultaneously combining ultra high optical finesse and high frequency vibrational modes. In the presently reported experiments we have overcome this limitation by microfabricating optimized silica toroidal whispering gallery mode (WGM) resonators which can accommodate the required high-quality optical and mechanical modes in one and the same device (Fig. 1b). The parameters $\Omega_m/2\pi = 73.5$ MHz and $F = 4.4 \cdot 10^5$, corresponding to $\kappa/2\pi = 3.2$ MHz, place the system system deeply into the resolved sideband regime. The repercussions of this regime on the cavity transmission are most strikingly observed when using an auxiliary laser

to drive the mechanical motion (using blue detuned light [3], cf. SI). Indeed, when tuning over the driven cavity, a series of optical resonances spaced by the mechanical frequencies can be observed, satisfying $\Omega_m/\kappa \approx 22$ (cf. Fig. 1c) which convincingly prove that the device satisfies the "strong binding" condition.

To demonstrate resolved sideband cooling, a grating-stabilized laser diode is coupled to a high-finesse whispering-gallery mode (WGM) near 970 nm of a second sample ($\Omega_m/2\pi = 40.6$ MHz, $\kappa/2\pi = 5.8$ MHz, $\Gamma_m/2\pi = 1.3$ kHz, $m_{\text{eff}} = 10$ ng), and locked to the first lower motional sideband (i.e. $\Delta = -\Omega_m$) using a frequency modulation technique and fast feedback (Fig. 2 a and SI). The cooling caused by this laser is independently and continuously monitored by a Nd:YAG laser ($\lambda = 1064$ nm) coupled to a different cavity mode. An adaptation of the Hänsch-Couillaud polarization spectroscopy technique to the present experiment (cf. SI), allows locking the monitoring laser to the centre of the resonance ($\Delta = 0$) which, in conjunction with low power levels, ensures that the readout laser's effect on the mechanical oscillator motion is negligible. Simultaneously, it provides a quantum-noise limited signal (cf. SI), which monitors the displacement noise of the cavity caused by the thermal excitation of the toroid's different mechanical modes (Fig. 3a,b). The sensitivity of this measurement reaches 10^{-18} m/ $\sqrt{\text{Hz}}$, which is among the best values achieved to date [30], and a value already sufficient to detect the zero-point mechanical motion $x_0 = \sqrt{\hbar/m_{\text{eff}}\Omega_m} \sim 10^{-16}$ m of typical radial breathing modes (RBMs).

Increasing the cooling laser power, a clear reduction of the displacement fluctuations is observed, characteristic of cooling. Note that our prior work has already demonstrated unambiguously that cooling in toroidal microcavities is *solely* due to radiation pressure [3, 4] and thermal contributions [31] play a negligible role. We thus observe, for the first time, resolved-sideband cooling of a micromechanical oscillator. Simultaneous measurements on other radially symmetric modes at lower frequencies reveal that these remain completely unaffected (Fig. 3c). This selectivity is specific to the regime of resolved sideband cooling, in contrast to the "weak binding" case, where the κ -wide absorption sidebands of different mechanical modes overlap. As shown in Fig. 3, the highest attained cooling rate $\Gamma_c/2\pi = 1.56$ MHz was achieved in the first sample ($\Omega_m/2\pi = 73.5$ MHz, $\kappa/2\pi = 3.2$ MHz). Note that of the 3 mW of launched power in the fibre only a fraction $\sim (4\tau^2\Omega_m^2 + 1)^{-1} \approx 5 \cdot 10^{-4}$ is coupled into the cavity (i.e. $1.5 \mu\text{W}$) due to the highly detuned laser. Combining such high cooling rates with the lowest achieved reservoir heating rates of $\Gamma_m = 1.3$ kHz it appears feasible to achieve a reduction of final (n_f) to initial (n_R) occupancy of $n_R/n_f \cong (\Gamma_c + \Gamma_m)/\Gamma_m > 10^3$. With the demonstrated $16\Omega_m^2/\kappa^2 = 7700$, this value would be sufficient to reach $n_f < 0.5$ when starting at a cryogenic temperature of 1.8 K, while still satisfying [22, 23] $n_R/n_f < Q_m$ and

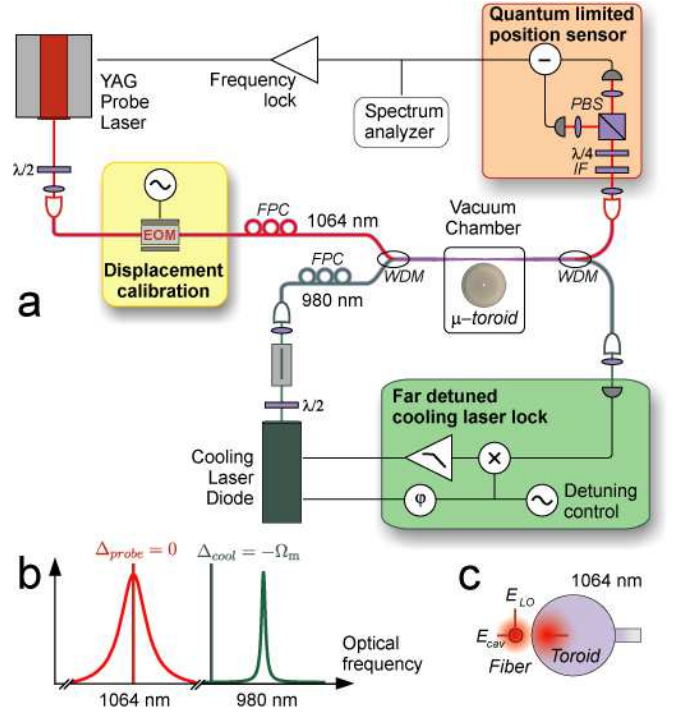


FIG. 2: Schematic of the experiment. **a** The opto-mechanical system (toroidal microcavity) is held in an evacuated chamber ($P < 10^{-1}$ mbar), and is simultaneously excited by a diode laser that serves for cooling and a Nd:YAG laser for quantum limited monitoring of the displacement of the cavity's mechanical modes. **b** By means of a frequency modulation technique, the cooling laser is locked far outside the cavity's WGM resonance to a detuning $\Delta = -\Omega_m$, while the monitoring laser is locked to the center of a different resonance using a variation of the Hänsch-Couillaud technique (cf. SI). **c** To this end, the monitoring laser is polarized such that only a small fraction of its power couples into the (polarization non-degenerate) WGM. The stronger orthogonal field component serves as a local oscillator in a polarization-sensitive detection scheme, giving rise to quantum noise limited displacement monitoring (cf. SI). The absolute calibration of the measured displacements is derived from a phase modulation of the probe laser with a known modulation depth (cf. SI). FPC: fiber polarization controller, WDM: wavelength division multiplexer, IF: interference filter, PBS: polarizing beam splitter, $\lambda/2$, $\lambda/4$: optical retarder plates.

$\Gamma_c < \kappa$. Starting from room temperature this would lead to $n_f < 100$. In the actual experiment, analysis of the *integrated* calibrated displacement noise spectra via the relation $n_f \hbar \Omega_m = \int m_{\text{eff}} \Omega S_x(\Omega) d\Omega$ indicates however significantly higher n_f . This discrepancy is attributed to heating by excess phase noise from the cooling laser, which was measured to be $\sqrt{S_\varphi} \approx 4 \mu\text{rad}/\sqrt{\text{Hz}}$ at radio frequencies close to Ω_m (cf. SI). The resulting radiation pressure noise limits the achievable occupancy to $n_{\text{min}} = \sqrt{2k_B T m_{\text{eff}} \Gamma_m S_\varphi R \Omega_m / \hbar \omega_0} \approx 5200$ for the parameters of the second sample, with which the lowest occupancies were achieved. Note that in this case the

(classical) correlations between the laser noise and the induced displacement fluctuations can cause "squashing" [32] artefacts if the diode laser were also used for mechanical readout. In contrast, the use of the independent Nd:YAG laser provides a faithful displacement monitor with which these induced fluctuations can be revealed. Such an analysis yields a final occupancy of $n_f \approx 5900$, in agreement with the above estimate.

A direct consequence of the resolved sideband regime is the strong suppression of motional increasing processes, which should lead to a significantly weaker red-sideband in the spectrum of the light emerging from the cavity (as analyzed in Ref [23]). To confirm this aspect, the motional sidebands generated during the cooling cycles were probed, similar to spectroscopy of the resonance fluorescence of a cooled ion [33]. This is achieved with a heterodyne experiment, by beating the cooling laser with a local oscillator (cf. Fig. 4a), derived by down-shifting part of the cooling laser light using an acousto-optic modulator at $\Omega_{\text{AOM}}/2\pi = 200$ MHz. The beat of the local oscillator and the cooling laser produces a modulation at Ω_{AOM} , while the motional sidebands signals now appear at $\Omega_{\text{AOM}} \pm \Omega_m$, thereby allowing the measurement of their individual weights. Figure 4b shows the result of this measurement for two different laser detunings. While for excitation on cavity line-center ($\Delta = 0$) the sideband intensities are equal (i. e. $\eta^2 A^- n \approx \eta^2 A^+ (n+1)$ since $n \gg 1$ and $A^- = A^+$), detuning the laser to the lower sideband $\Delta = \Omega_m$ should lead to a strong suppression of the red sideband beat by a factor of A^-/A^+ . In the experiment with the 40.6-MHz sample, the detuning is chosen such that the red sideband is still discernible above the laser noise, corresponding to a suppression of 16 dB, providing an independent confirmation that cooling occurs in the resolved sideband regime. Optimizing the laser detuning, the red emission sideband could be reduced even further. It is important to note that the ability to measure the individual sidebands separately as demonstrated here is important for future experiments which venture in the quantum regime. As theoretically predicted [22, 23]—and in analogy to trapped ions [10]—the weights of the sidebands allow inferring the average motional occupation number [23] for low occupancies by measuring the ratio of the red and blue sidebands.

The regime of resolved sidebands has another important—and counterintuitive—benefit, since the cooling rate is indeed higher in comparison to the unresolved case. Keeping the launched power P as well as Ω_m and R fixed, an increase in the cavity finesse increases the cooling rate, until it saturates in the highly resolved sideband case and approaches an asymptotic value (cf. SI). The *circulating* power however continues to decrease, mitigating undesired effects such as photo-thermal or radiation pressure induced bi-stability or absorption induced heating. It is important to note however, that the final occupancies for very high optical fi-

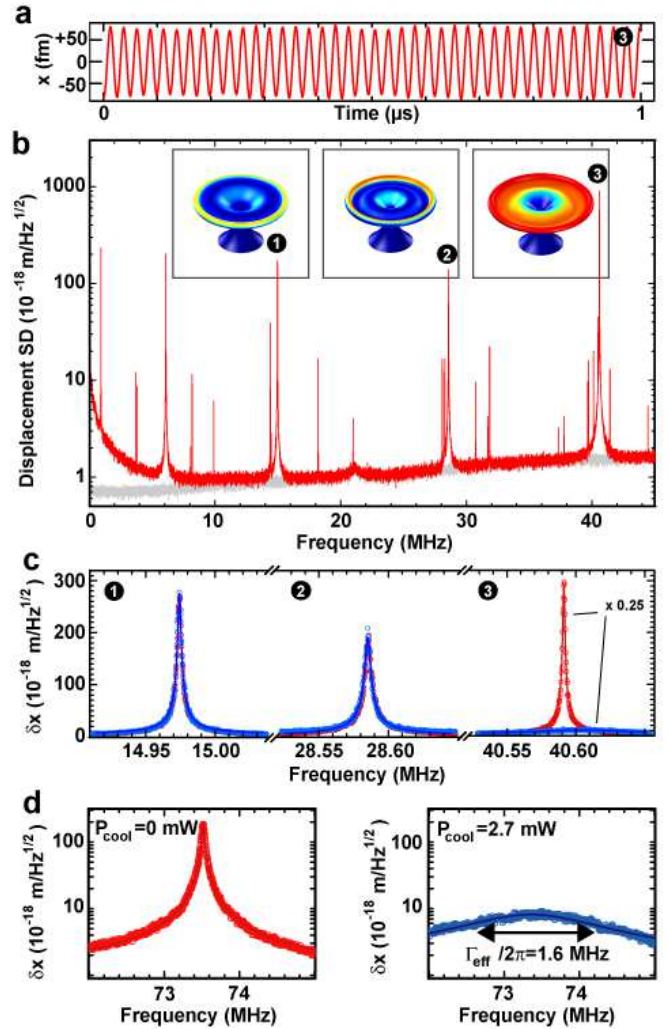


FIG. 3: Resolved sideband cooling of the radial breathing mode. **a** Time-domain trace of the Brownian motion of the radial breathing mode as observed by the monitoring laser in a 2 MHz spectral bandwidth around $\Omega_m/2\pi = 40.6$ MHz. **b** Full spectrum of the displacement noise at room temperature, recorded with the Nd:YAG laser (red). The different peaks appearing in the spectrum represents the mechanical eigenmodes which can be identified using three-dimensional finite-element analysis. The modes denoted by (1,2,3) are rotationally symmetric mechanical modes, whose strain (colour code) and deformed shapes are shown in the insets. The background of the measurement (gray) is due to shot noise, its frequency dependence results from the reduced displacement sensitivity (for the same measured noise level) at frequencies exceeding the cavity's bandwidth. A signal-to-background ratio close to 60 dB is achieved at room temperature. **c** Resolved sideband cooling with the cooling laser tuned to the lower sideband of the radially symmetric radial breathing mode (3). As evident only mode (3) is cooled while all other modes (of which (1) and (2) are shown) remain unaffected. Circles represent noise spectra with the cooling laser off (red) and running at $300 \mu\text{W}$ (blue). Lines are Lorentzian fits. **d** Cooling rates exceeding 1.5 MHz obtained with the 73.5-MHz RBM of a different sample.

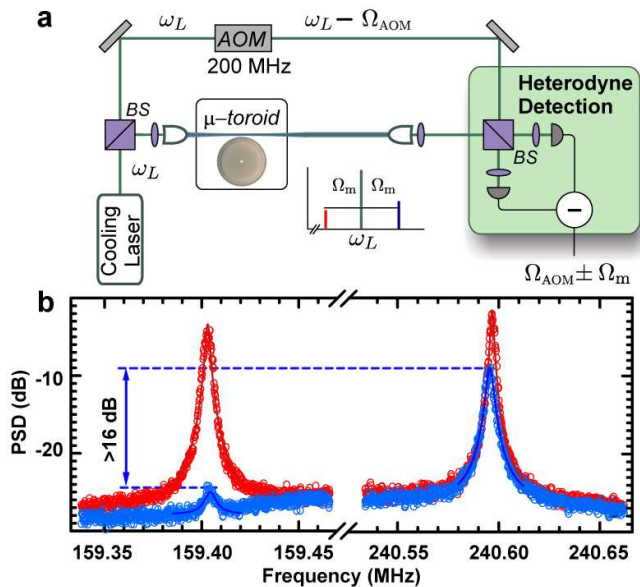


FIG. 4: Motional sideband spectroscopy. **a** Experimental setup used to resolve upper and lower motional sideband generated during interaction of the cooling laser with the cavity, similar to the spectroscopy of the resonance fluorescence of a laser-cooled ion [33]. The cooling laser interacts with the optical microcavity whose transmission is subsequently superimposed with a second laser beam retrieved from the same cooling laser but down-shifted by 200 MHz using an acousto-optic modulator (AOM). The beating of the two signals is recorded using a balanced heterodyne detector, yielding spectral components of the lower (upper) sideband at $200 \text{ MHz} - \Omega_m/2\pi$ ($200 \text{ MHz} + \Omega_m/2\pi$). **b** Beat signals of the upper (anti-Stokes) and lower (Stokes) motional sideband, for $\Delta = 0$ (red) and a detuning close to $\Delta = -\Omega_m$ (blue). The plotted electrical power spectral density (PSD) is proportional to the optical PSD in the sidebands. For zero detuning of the pump with respect to the optical cavity the motional sidebands are equal in power. By tuning the laser to the lower sideband, which induced cooling, 40-fold (16 dB) reduction of the Stokes sideband is observed as required for achieving ground state cooling.

nesses are bound by the maximum entropy flow which is given by the cavity decay rate [22], i.e. $n_R/n_f < \kappa/\Gamma_m$.

Pertaining to the wider implications of our work, we note that resolved sideband cooling as demonstrated here, is a key prerequisite for ground state cooling and is an enabling step toward observing quantum mechanical phenomena of macroscopic objects [8, 9] such as the generation of non-classical states of motion. The regime of resolved sidebands is also a prerequisite to a “continuous two transducer measurement” scheme [25] which allows exceeding the standard quantum limit by $\sqrt{\Omega_m/\kappa}$, a factor of ca. 5 for the parameters reported here. Along these lines, continuous QND measurements of a mechanical oscillator should produce squeezed states of mechanical motion.

The authors acknowledge discussions with T. W.

Hänsch, W. Zwerger and I. Wilson-Rae. TJK acknowledges support via an Independent Max Planck Junior Research Group Grant, a Marie Curie Excellence Grant (JRG-UHQ), the DFG funded Nanoscience Initiative Munich (NIM) and a Marie Curie Reintegration Grant (RG-UHQ). The authors gratefully acknowledge J. Kotthaus for access to clean-room facilities for micro-fabrication.

* Electronic address: tjk@mpq.mpg.de

- [1] O. Arcizet, P.-F. Cohadon, T. Briant, M. Pinard, and A. Heidmann, *Nature* **444**, 71 (2006).
- [2] S. Gigan, H. R. Böhm, M. Paternosto, F. Blaser, G. Langer, J. B. Hertzberg, K. C. Schwab, D. Bäuerle, M. Aspelmeyer, and A. Zeilinger, *Nature* **444**, 67 (2006).
- [3] T. J. Kippenberg, H. Rokhsari, T. Carmon, A. Scherer, and K. J. Vahala, *Physical Review Letters* **95**, 033901 (2005).
- [4] A. Schliesser, P. Del’Haye, N. Nooshi, K. Vahala, and T. Kippenberg, *Physical Review Letters* **97**, 243905 (2006).
- [5] T. Corbitt, Y. Chen, E. Innerhofer, H. Müller-Ebhardt, D. Ottaway, H. Rehbein, D. Sigg, S. Whitcomb, C. Wipf, and N. Mavalvala, *Physical Review Letters* **98**, 150802 (2007).
- [6] P.-F. Cohadon, A. Heidmann, and M. Pinard, *Physical Review Letters* **83**, 3174 (1999).
- [7] V. B. Braginsky, S. E. Strigin, and V. P. Vyatchanin, *Physics Letters A* **287**, 331 (2001).
- [8] K. C. Schwab and M. L. Roukes, *Physics Today* **58**, 36 (2005).
- [9] S. Mancini, V. Giovannetti, D. Vitali, and P. Tombesi, *Physical Review Letters* **88**, 120401 (2002).
- [10] F. Diedrich, J. C. Bergquist, W. M. Itano, and D. J. Wineland, *Phys. Rev. Lett.* **62**, 403 (1989).
- [11] C. Monroe, D. M. Meekhof, B. E. King, S. R. Jefferts, W. M. Itano, D. J. Wineland, and P. Gould, *Physical Review Letters* **75**, 4011 (1995).
- [12] A. D. Boozer, A. Boca, R. Miller, T. E. Northup, and H. J. Kimble, *Physical Review Letters* **97**, 083602 (2006).
- [13] S. E. Hamann, D. L. Haycock, G. Klose, P. H. Pax, I. H. Deutsch, and P. S. Jessen, *Physical Review Letters* **80**, 4149 (1998).
- [14] D. M. Meekhof, C. Monroe, B. E. King, W. M. Itano, and D. J. Wineland, *Physical Review Letters* **76**, 1796 (1996).
- [15] C. Monroe, D. M. Meekhof, B. E. King, and D. J. Wineland, *Science* **272**, 1131 (1996).
- [16] H. G. Dehmelt, *Nature* **262**, 777 (1976).
- [17] D. J. Wineland and H. Dehmelt, *Bulletin of the American Physical Society* **20**, 637 (1975).
- [18] W. Neuhauser, M. Hohenstatt, P. Toschek, and H. Dehmelt, *Phys. Rev. Lett.* **41**, 233 (1978).
- [19] D. J. Wineland and W. M. Itano, *Physical Review A* **20**, 1521 (1979).
- [20] V. B. Braginsky and S. P. Vyatchanin, *Physics Letters A* **293**, 228 (2002).
- [21] K. Karrai, *Nature* **444**, 41 (2006).
- [22] F. Marquardt, J. P. Chen, A. A. Clerk, and S. M. Girvin,

- Physical Review Letters **99**, 093902 (2007).
- [23] I. Wilson-Rae, N. Nooshi, W. Zwerger, and T. J. Kippenberg, Physical Review Letters **99**, 093901 (2007).
- [24] D. K. Armani, T. J. Kippenberg, S. M. Spillane, and K. J. Vahala, Nature **421**, 925 (2003).
- [25] V. B. Braginsky and F. Y. Khalili, *Quantum Measurement* (Cambridge University Press, 1992).
- [26] D. Leibfried, R. Blatt, C. Monroe, and D. Wineland, Review of Modern Physics **75**, 281 (2003).
- [27] L. Tian and P. Zoller, Physical Review Letters **93**, 266403 (2004).
- [28] I. Wilson-Rae, P. Zoller, and A. Imamoglu, Physical Review Letters **92**, 075507 (2004).
- [29] S. Stenholm, Reviews of Modern Physics **58**, 699 (1986).
- [30] O. Arcizet, P.-F. Cohadon, T. Briant, M. Pinard, A. Heidmann, J.-M. Mackowski, C. Michel, L. Pinard, O. Francais, and L. Rousseau, Physical Review Letters **97**, 133601 (2006).
- [31] C. Hühberger Metzger and K. Karrai, Nature **432**, 1002 (2004).
- [32] M. Poggio, L. Degen, J. J. Mamin, and D. Rugar, Physical Review Letters **99**, 017201 (2007).
- [33] C. Raab, J. Eschner, J. Bolle, H. Oberst, F. Schmidt-Kaler, and R. Blatt, Physical Review Letters **85**, 538 (2000).
- [34] D. C. Bjorklund, M. D. Levenson, W. Lenth, and C. Ortiz, Applied Physics B **32**, 145 (1983).
- [35] H. A. Haus, *Waves and fields in optoelectronics* (Prentice-Hall, 1984).
- [36] T. Carmon, L. Yang, and K. J. Vahala, Optics Express **12**, 4742 (2004).
- [37] T. W. Hänsch and B. Couillaud, Optics Communications **35**, 441 (1980).
- [38] T. C. Zhang, J. P. Poizat, et al., Quantum and semiclassical optics **7**, 601 (1995).
-

SAMPLE PREPARATION

Silica microtoroids are fabricated from thermally grown oxide on a silicon chip by a combination of wet- and dry-etching with a CO₂ reflow technique as detailed in prior work [24]. Upon completion of these initial steps, the silicon pillar supporting the toroid is re-etched until sub-micron tip diameters are reached in order to decouple the toroid's mechanical mode from the substrate, yielding quality factors of 30,000 for the radial breathing mode. Under appropriate conditions, no degradation of the optical modes is observed in this step. Since the Nd:YAG laser has only a limited tuning range, the toroid is subsequently subjected to repeated low-dose radiation from a CO₂ laser to evaporate minute layers of toroid material, until a suited WGM is tuned into the range accessible with the Nd:YAG laser. The diode laser is then tuned to a WGM with an ultra high finesse ($> 10^5$) and negligible mode splitting.

LOCKING OF THE COOLING LASER

To achieve resolved sideband cooling, the cooling laser, a grating-stabilized diode laser, has to be locked far-detuned from the WGM resonance. To this end, it is frequency-modulated by applying a small rf modulation of frequency Ω_{mod} to the current across the diode. Similar to the Pound-Drever-Hall (PDH) method, the resulting amplitude modulation of the light transmitted by the cavity is demodulated with a phase chosen to obtain an absorptive error signal [34]. This creates a steep error signal at detunings corresponding to a mechanical mode's eigenfrequency Ω_{m} , while not applying a phase modulation resonant with the mechanical mode. Typically, a modulation frequency of $\Omega_{\text{mod}} = \Omega_{\text{m}} - \kappa/2$ is chosen, such that effectively a modulation sideband of the laser is locked to the red wing of the WGM resonance, while the laser carrier pumps the motional sideband at $\Delta = -\Omega_{\text{m}}$. To lock the laser, the error signal is offset to choose the appropriate detuning, and fed to slow and fast feedback branches, respectively actuating the grating and the pump current in the diode.

COOLING RATE

For the ring topology of the considered optomechanical system, the cooling rate in the regime $\Gamma_{\text{c}} < \kappa$ can generally be written as [4]

$$\Gamma_{\text{c}} = \frac{8F^2 n^2 \omega_0}{m_{\text{eff}} c^2 \Omega_{\text{m}}} \frac{1/\kappa \tau_{\text{ex}}}{4\Delta^2/\kappa^2 + 1} \left(\frac{1}{4(\Delta + \Omega_{\text{m}})^2/\kappa^2 + 1} - \frac{1}{4(\Delta - \Omega_{\text{m}})^2/\kappa^2 + 1} \right) P. \quad (\text{S1})$$

Here F is finesse, n the refractive index, ω_0 optical resonance frequency, m_{eff} the effective mass, c vacuum light speed, Ω_{m} mechanical resonance frequency, κ cavity linewidth and therefore inverse total photon lifetime, τ_{ex} photon lifetime due to coupling, Δ detuning and P launched power. All frequencies are in angular frequency units. Using the finesse of a circular resonator $F = c/nR\kappa$ and a fixed coupling parameter $K \equiv 1/(\kappa\tau_{\text{ex}} - 1)$, this can be re-written as

$$\Gamma_{\text{c}} = \frac{\omega_0}{\Omega_{\text{m}}} \frac{1}{m_{\text{eff}} R^2} \frac{K}{2(K+1)} \frac{\kappa^2}{\Delta^2 + (\kappa/2)^2} \left(\frac{1}{(\Delta + \Omega_{\text{m}})^2 + (\kappa/2)^2} - \frac{1}{(\Delta - \Omega_{\text{m}})^2 + (\kappa/2)^2} \right) P. \quad (\text{S2})$$

Keeping all other parameters other than κ and Δ fixed, it is easy to show that this expressions reaches a maximum for $\Delta = -\Omega_{\text{m}}$ and $\kappa \rightarrow 0$,

$$\Gamma_{\text{c}}^{\text{max}} = \frac{\omega_0}{\Omega_{\text{m}}^3} \frac{1}{m_{\text{eff}} R^2} \frac{2K}{K+1} P. \quad (\text{S3})$$

The resolved sideband regime is *per se* most ideally suited for backaction cooling (Fig. S1), provided the linewidth is reduced without changing the cavity radius (or length), i.e. by increasing finesse.

TRANSMISSION OF AN OSCILLATING CAVITY

Assume the cavity is oscillating such that its radius is sinusoidally displaced by

$$x(t) = x_0 \sin(\Omega_{\text{m}} t). \quad (\text{S4})$$

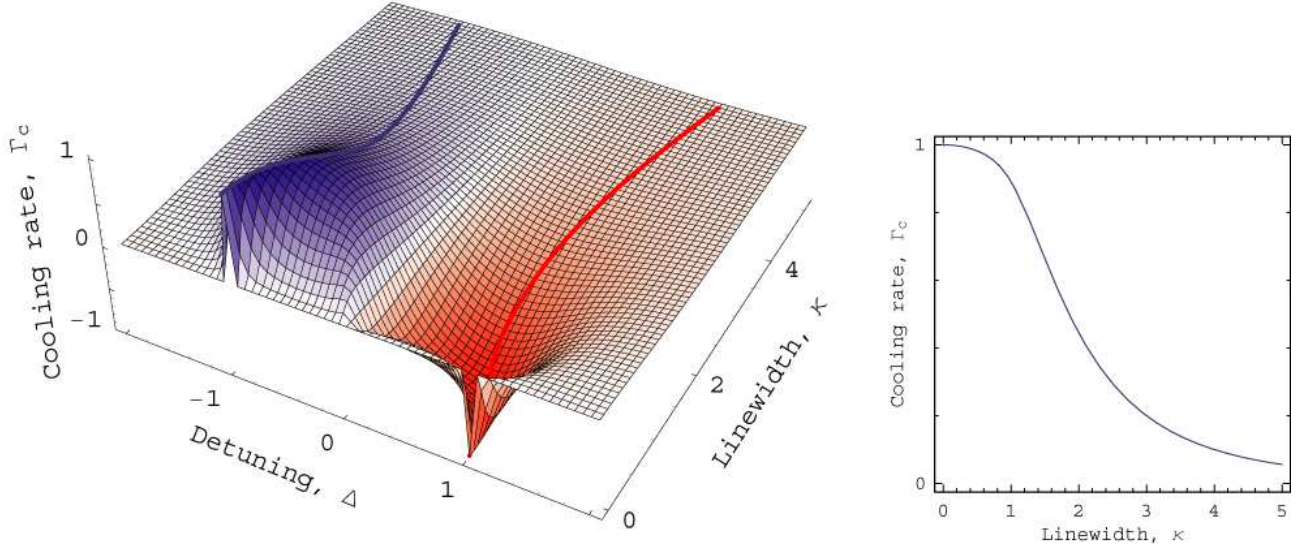


FIG. S1: Left: Cooling rate Γ_c , normalized to Γ_c^{\max} , as a function of detuning Δ and cavity linewidth κ , where a mechanical resonance frequency $\Omega_m \equiv 1$ was assumed. Thick blue and red lines trace the detunings which provide maximum (blue) or minimum (red) cooling rates for a given linewidth. Right: Normalized cooling rate achievable for a given linewidth κ (with $\Omega_m \equiv 1$) when the optimum detuning is chosen.

In the framework of coupled-mode theory [35], its intracavity mode amplitude a is described by

$$\dot{a}(t) = \left(-\frac{\kappa}{2} + i\omega_0 \left(1 - \frac{x(t)}{R} \right) \right) a(t) + \frac{s}{\sqrt{\tau_{\text{ex}}}} e^{i\omega t} \quad (\text{S5})$$

where $|a|^2$ is normalized to the intracavity energy, $|s|^2$ normalized to the incident power, ω_0 the cavity resonance frequency, ω the driving laser frequency, R the mean radius of the cavity, τ_{ex} the lifetime due to coupling and κ the FWHM linewidth of the cavity in angular frequencies and equal to the inverse total photon lifetime.

The homogeneous solution of the ordinary differential equation (S5) reads

$$a_h(t) = A_0 \exp \left(\left(-\frac{\kappa}{2} + i\omega_0 \right) t + i \frac{x_0 \omega_0}{R \Omega_m} \cos(\Omega_m t) \right) \quad (\text{S6})$$

with a boundary-condition dependent A_0 . One particular solution may have the form $a_p(t) = A(t)a_h(t)$, satisfying

$$\dot{A}(t) = \frac{s}{\sqrt{\tau_{\text{ex}}}} \exp \left(\left(\frac{\kappa}{2} - i\omega_0 \right) t - i \frac{x_0 \omega_0}{R \Omega_m} \cos(\Omega_m t) + i\omega t \right). \quad (\text{S7})$$

Introducing the modulation index

$$\beta \equiv \frac{x_0 \omega_0}{R \Omega_m} \quad (\text{S8})$$

the expansion of the cosine argument into Bessel functions $\exp(-i\beta \cos(\Omega_m t)) = \sum_{n=-\infty}^{+\infty} (-i)^n J_n(\beta) \exp(in\Omega_m t)$ allows straightforward integration of (S7), yielding, with $\Delta \equiv \omega - \omega_0$,

$$a_p(t) = \frac{s}{\sqrt{\tau_{\text{ex}}}} \sum_{n=-\infty}^{+\infty} \frac{(-i)^n J_n(\beta)}{\kappa/2 + i(\Delta + n\Omega_m)} \exp(i(\omega + n\Omega_m)t + i\beta \cos(\Omega_m t)). \quad (\text{S9})$$

The general solution $a(t) = a_h(t) + a_p(t)$ of eq. (S5) converges towards $a_p(t)$ on a timescale of $2/\kappa$ for all A_0 , since $a_h(t) \propto \exp(-\kappa t/2)$, so that the steady state solution is given by a_p . The field transmitted through the taper past

the cavity is given by $s_{\text{out}} = se^{i\omega t} - a_p/\sqrt{\tau_{\text{ex}}}$ and the transmitted power is

$$|s_{\text{out}}|^2 = \left| se^{i\omega t} - \frac{a_p}{\sqrt{\tau_{\text{ex}}}} \right|^2 = |s|^2 - 2\text{Re} \left\{ s^* e^{-i\omega t} \cdot \frac{a_p}{\sqrt{\tau_{\text{ex}}}} \right\} + \frac{|a_p|^2}{\tau_{\text{ex}}} \quad (\text{S10})$$

with

$$-2\text{Re} \left\{ s^* e^{-i\omega t} \cdot \frac{a_p}{\sqrt{\tau_{\text{ex}}}} \right\} = -2 \frac{|s|^2}{\tau_{\text{ex}}} \text{Re} \left\{ \sum_{n,m} \frac{i^{m-n} J_n(\beta) J_m(\beta) \exp(i(n+m)\Omega_m t)}{\kappa/2 + i(\Delta + n\Omega_m)} \right\} \quad (\text{S11})$$

and

$$\frac{|a_p|^2}{\tau_{\text{ex}}} = \frac{|s|^2}{\tau_{\text{ex}}^2} \left| \sum_{n,m} \frac{i^{n-m} J_n(\beta) J_m(\beta) e^{i(n-m)\Omega_m t}}{(\kappa/2 + i(\Delta + n\Omega_m))(\kappa/2 - i(\Delta + m\Omega_m))} \right|^2. \quad (\text{S12})$$

If only the DC signal is detected, only the terms with $m = -n$ in (S11) and $m = n$ in (S12) have to be considered. Then

$$|s_{\text{out}}^{\text{DC}}|^2 = |s|^2 \left(1 - 2 \frac{1}{\tau_{\text{ex}}} \text{Re} \left\{ \sum_n \frac{J_n(\beta)^2}{\kappa/2 + i(\Delta + n\Omega_m)} \right\} + \frac{1}{\tau_{\text{ex}}^2} \sum_n \frac{J_n(\beta)^2}{(\kappa/2)^2 + (\Delta + n\Omega_m)^2} \right) = \quad (\text{S13})$$

$$= |s|^2 \left(1 - \frac{K\kappa^2}{(1+K)^2} \sum_n \frac{J_n(\beta)^2}{(\kappa/2)^2 + (\Delta + n\Omega_m)^2} \right). \quad (\text{S14})$$

Therefore, the DC signal consists of a series of Lorentzian dips at frequencies $\omega_0 + n\Omega_m$, the width of which is given by the normal cavity linewidth κ . The depth of the dips reflects the coupling conditions, while the modulation index $\beta = x_0\omega_0/R\Omega_m$ determines the relative weights of the sidebands.

In the experiment, both the diode and the Nd:YAG laser are coupled simultaneously to the cavity, as described in Fig. 2 of the manuscript. The Nd:YAG laser is however locked to the blue wing of the WGM resonance, and a power sufficient to exceed the threshold for the parametric oscillation instability is sent to the cavity. The diode laser is then scanned over several hundred megahertz in the frequency region of another WGM resonance. To enhance the signal-to-noise ratio also for very low powers (at which thermal nonlinearities [36] are sufficiently well suppressed), a lock-in technique is employed. The side-dips disappeared when the Nd:YAG laser was switched off and their relative weights changed with the detuning of this laser. From the fitted modulation depths of $\beta = (0.94, 1.47, 1.75)$ oscillation amplitudes of $x_0 = (5.4, 8.4, 10.0)$ pm can be inferred. For comparison, a displacement of 25 pm would shift the cavity resonance frequency by one linewidth.

DISPLACEMENT READOUT

Implementation

Adapting the Hänsch-Couillaud polarization spectroscopy technique [37], a dispersive error signal is created by probing the ellipticity in polarization which is introduced to the light propagating in the taper, when part of the light (\vec{E}_{cav}) couples into one of the (polarization non-degenerate) WGM of the microtoroid. The polarization component which does not interact with the cavity (\vec{E}_{LO}) thus essentially serves as a reference for the phase shift introduced by the cavity. Sufficiently strong, it can be used as a local oscillator, boosting all optical noises above the detector noise.

The polarization analyzer consists only of a $\lambda/4$ -retarder plate, rotated to an angle of 45° with respect to the subsequent polarizing beam splitter (PBS). The two detected signals represent a decomposition of the elliptically polarized light into a basis of left- and right-handed circular polarizations. The difference of these two signals therefore indicates the handedness of the incoming polarization state, which indicates the respective detuning of the laser from the WGM's line center. In addition to this scheme [37], in the experiment described here, polarization mode dispersion (PMD) in the optical fibre has to be compensated by introducing an additional pair of $\lambda/4$ - and $\lambda/2$ -retarder plates before the polarization analyzer (not shown in schematic Fig. 2 of the manuscript).

The complex transfer function of the taper for the cavity polarization component is given by [35]

$$t(\Delta) \cdot E_{\text{cav}} = \frac{\tau_{\text{ex}} - \tau_0 + 2i\Delta\tau_0\tau_{\text{ex}}}{\tau_{\text{ex}} + \tau_0 + 2i\Delta\tau_0\tau_{\text{ex}}} \cdot E_{\text{cav}} \quad (\text{S15})$$

where τ_0 is the intrinsic photon lifetime and τ_{ex} the lifetime due to coupling with $\kappa \equiv \tau_0^{-1} + \tau_{\text{ex}}^{-1}$. Using Jones matrices C_Δ , Q , H , R_θ , P for the effect of the cavity, quarter- and half-waveplate, a basis rotation and polarization mode dispersion, the detected fields l , r on the two photodiodes are

$$\begin{pmatrix} l \\ r \end{pmatrix} = R_{\theta_4}(R_{\theta_3}^{-1}QR_{\theta_3})(R_{\theta_2}^{-1}HR_{\theta_2})(R_{\theta_1}^{-1}QR_{\theta_1})PC_\Delta \cdot \begin{pmatrix} E_{\text{cav}} \\ E_{\text{LO}} \end{pmatrix}. \quad (\text{S16})$$

Adjusting the angles θ_i , P can be compensated such that effectively

$$\begin{pmatrix} l \\ r \end{pmatrix} = R_{45^\circ}QC_\Delta \cdot \begin{pmatrix} E_{\text{cav}} \\ E_{\text{LO}} \end{pmatrix} = \frac{1}{\sqrt{2}} \begin{pmatrix} 1 & 1 \\ -1 & 1 \end{pmatrix} \begin{pmatrix} 1 & 0 \\ 0 & i \end{pmatrix} \begin{pmatrix} t(\Delta) & 0 \\ 0 & 1 \end{pmatrix} \begin{pmatrix} E_{\text{cav}} \\ E_{\text{LO}} \end{pmatrix} = \frac{1}{\sqrt{2}} \begin{pmatrix} t(\Delta)E_{\text{cav}} + iE_{\text{LO}} \\ -t(\Delta)E_{\text{cav}} + iE_{\text{LO}} \end{pmatrix} \quad (\text{S17})$$

Sensitivity

In the case of displacements slow enough so that intracavity power can adiabatically follow, the Hänsch-Couillaud error signal $h(\Delta) = |l|^2 - |r|^2$ reads

$$h(\Delta) = \frac{8\tau_0^2\tau_{\text{ex}}\Delta}{\tau_{\text{ex}}^2 + 2\tau_0\tau_{\text{ex}} + \tau_0^2(1 + 4\Delta^2\tau_{\text{ex}}^2)} \sqrt{P_{\text{cav}}P_{\text{LO}}}. \quad (\text{S18})$$

If the cavity is probed on resonance $\omega - \omega_0 \equiv 0$, small displacements x from an original resonator radius R will cause a detuning of $\Delta = \omega_0 x/R$ and therefore a signal of

$$\left. \frac{\partial}{\partial x} h(\omega_0 x/R) \right|_{x=0} \cdot x = \frac{8\omega_0}{\tau_{\text{ex}}\kappa^2 R} \sqrt{P_{\text{cav}}P_{\text{LO}}} \cdot x \quad (\text{S19})$$

can be expected. In the case of critical coupling $\tau_{\text{ex}} = 2/\kappa$ and for a strong local oscillator $P_{\text{LO}} \gg P_{\text{cav}}$, the local oscillator's shot noise in the differential signal $\sqrt{2}\sqrt{\eta P_{\text{LO}}/2}/(\hbar\omega)$ can be used to estimate the shot-noise limited sensitivity to

$$x_{\text{min}} = \frac{\lambda}{8\pi\mathcal{F}\sqrt{\eta P_{\text{cav}}/(\hbar\omega)}}, \quad (\text{S20})$$

with the (ring) resonator finesse $\mathcal{F} = c/\kappa nR$ and the intracavity laser wavelength $\lambda = 2\pi c/n\omega$. Assuming shot-noise limited operation, typical parameters $\mathcal{F} = 40,000$, $\eta = 0.5$, $P_{\text{cav}} = 1\mu\text{W}$ and $\lambda = 1064\text{nm}/1.4$ already yield a sensitivity of $x_{\text{min}} = 5 \cdot 10^{-19}\text{m}/\sqrt{\text{Hz}}$.

We have confirmed experimentally that the readout laser is shot-noise limited, and that the electronic noise in the detection system is overwhelmed by the laser noise by more than 10 dB at all frequencies of interest.

It is important to consider the response of the Hänsch-Couillaud signal also at frequencies exceeding the cavity bandwidth for measurements on high-frequency mechanical modes. Assuming small displacement fluctuations $\beta = x_0\omega_0/R\Omega \ll 1$ at Fourier frequency Ω , the expression (S9) for the intracavity field can be expanded in β and only terms in zeroth and first order in β retained:

$$a_{\text{p}}(t) = a_0(t) + \mathcal{O}(\beta^1) = a_0(t) + a_1(t) + \mathcal{O}(\beta^2) = \dots \quad (\text{S21})$$

with

$$a_0(t) = \frac{se^{i\omega t}}{\sqrt{\tau_{\text{ex}}}} \frac{J_0(\beta)^2}{\kappa/2 + i\Delta} \quad (\text{S22})$$

$$\begin{aligned} a_1(t) &= \frac{se^{i\omega t}}{\sqrt{\tau_{\text{ex}}}} \left(\left(\frac{-iJ_1(\beta) \exp(+i\Omega_{\text{m}}t)}{\kappa/2 + i(\Delta + \Omega_{\text{m}})} + \frac{iJ_{-1}(\beta) \exp(-i\Omega_{\text{m}}t)}{\kappa/2 + i(\Delta - \Omega_{\text{m}})} \right) \cdot J_0(\beta) + \right. \\ &\quad \left. + \frac{J_0(\beta)}{\kappa/2 + i\Delta} \cdot (iJ_1(\beta) \exp(+i\Omega_{\text{m}}t) - iJ_{-1}(\beta) \exp(-i\Omega_{\text{m}}t)) \right) = \end{aligned} \quad (\text{S23})$$

$$= \frac{se^{i\omega t}}{\sqrt{\tau_{\text{ex}}}} \frac{J_0(\beta)J_1(\beta)\Omega_{\text{m}}}{\kappa/2 + i\Delta} \left(-\frac{\exp(+i\Omega_{\text{m}}t)}{\kappa/2 + i(\Delta + \Omega_{\text{m}})} + \frac{\exp(-i\Omega_{\text{m}}t)}{\kappa/2 + i(\Delta - \Omega_{\text{m}})} \right) \quad (\text{S24})$$

Using $J_0(\beta) \cong 1$ and $J_1(\beta) \cong \beta/2$ for small β and the definition (S8), one finds

$$a(t) \cong \frac{E_{\text{cav}}}{\sqrt{\tau_{\text{ex}}}} \left(\frac{1}{\kappa/2 + i\Delta} - \frac{x}{R} \frac{\omega_0}{2} \frac{1}{\kappa/2 + i\Delta} \left(\frac{\exp(+i\Omega t)}{\kappa/2 + i(\Delta + \Omega)} - \frac{\exp(-i\Omega t)}{\kappa/2 + i(\Delta - \Omega)} \right) \right). \quad (\text{S25})$$

The detected fields behind the polarization analyzer are

$$\begin{pmatrix} l \\ r \end{pmatrix} = R_{45^\circ} \cdot Q \cdot \begin{pmatrix} -a/\sqrt{\tau_{\text{ex}}} + E_{\text{cav}} \\ E_{\text{LO}} \end{pmatrix} = \frac{1}{\sqrt{2}} \begin{pmatrix} -a/\sqrt{\tau_{\text{ex}}} + E_{\text{cav}} + iE_{\text{LO}} \\ a/\sqrt{\tau_{\text{ex}}} - E_{\text{cav}} + iE_{\text{LO}} \end{pmatrix}. \quad (\text{S26})$$

If the readout laser is locked to line center, $\omega = \omega_0$, the signal on one photodiode reads

$$|l|^2 = \frac{1}{2} \left| -\frac{E_{\text{cav}}}{\tau_{\text{ex}}} \frac{2}{\kappa} \left(1 - \frac{x_0}{R} \frac{\omega_0}{2} \left(\frac{e^{+i\Omega t}}{\kappa/2 + i\Omega} - \frac{e^{-i\Omega t}}{\kappa/2 - i\Omega} \right) \right) + E_{\text{cav}} + iE_{\text{LO}} \right|^2, \quad (\text{S27})$$

for a strong local oscillator $|E_{\text{LO}}| \gg |E_{\text{cav}}|$ (and rigorously for critical coupling $\tau_{\text{ex}} = 2/\kappa$) simplifying to

$$\cong |l_{\text{DC}}^2 - \frac{1}{2} \cdot 2\text{Re} \left\{ i \frac{E_{\text{LO}} E_{\text{cav}}}{\tau_{\text{ex}}} \frac{2}{\kappa} \frac{x_0}{R} \frac{\omega_0}{2} \left(\frac{e^{+i\Omega t}}{\kappa/2 + i\Omega} - \frac{e^{-i\Omega t}}{\kappa/2 - i\Omega} \right) \right\} = \quad (\text{S28})$$

$$= |l_{\text{DC}}^2 + \frac{\sqrt{P_{\text{LO}} P_{\text{cav}}}}{\tau_{\text{ex}}} \frac{2}{\kappa} \frac{x_0}{R} \omega_0 \frac{(\kappa/2) \sin(\Omega t) - \Omega \cos(\Omega t)}{(\kappa/2)^2 + \Omega^2} \quad (\text{S29})$$

An analogous calculation for r yields

$$h(t) = 2 \frac{\sqrt{P_{\text{LO}} P_{\text{cav}}}}{\tau_{\text{ex}}} \frac{2}{\kappa} \frac{x_0}{R} \omega_0 \frac{(\kappa/2) \sin(\Omega t) - \Omega \cos(\Omega t)}{(\kappa/2)^2 + \Omega^2}, \quad (\text{S30})$$

reproducing the adiabatic response in the corresponding limit $\Omega \ll \kappa/2$. This modulated optical power generates a modulated (differential) photocurrent $I = e\eta h/(\hbar\omega)$. After amplification by a transimpedance amplifier of gain $g[V/A]$, the *power* $P_{\text{rf}} = |gI|^2/R_{\text{term}}$ (with R_{term} the termination resistance) of the radio-frequency signal is spectrally analyzed. Then the sine and cosine terms add in quadrature, and

$$P_{\text{rf}}(\Omega) \propto \frac{(\kappa/2)^2 + \Omega^2}{((\kappa/2)^2 + \Omega^2)^2} = \frac{1}{(\kappa/2)^2 + \Omega^2}. \quad (\text{S31})$$

This reduced response of the readout signal has to be considered when the measured photocurrent spectral density is converted to a displacement spectral density. It is also the reason why the shot-noise limited sensitivity is not flat in Fourier frequencies, instead it scales as

$$x_{\text{min}}(\Omega) = \frac{\lambda}{8\pi\mathcal{F}\sqrt{\eta P_{\text{cav}}/(\hbar\omega)}} \sqrt{1 + \frac{\Omega^2}{(\kappa/2)^2}}. \quad (\text{S32})$$

Calibration

To calibrate the measured displacements, the light of the readout laser is phase-modulated using an electro-optic modulator. If the modulation depth is $\delta\varphi$ and the modulation frequency Ω , the field sent to the cavity can approximately written as $E_{\text{cav}}(1 + \frac{\delta\varphi}{2}e^{i\Omega t} - \frac{\delta\varphi}{2}e^{-i\Omega t})$ and the local oscillator, *which also gets modulated*, as $E_{\text{LO}}(1 + \frac{\delta\varphi}{2}e^{i\Omega t} - \frac{\delta\varphi}{2}e^{-i\Omega t})$. The field detected by one photodiode then reads

$$\begin{aligned} l = \frac{1}{\sqrt{2}} & \left(\left(1 - \frac{1}{\tau_{\text{ex}}} \frac{1}{\kappa/2 + i\Delta} \right) E_{\text{cav}} + \frac{\delta\varphi}{2} \left(1 - \frac{1}{\tau_{\text{ex}}} \frac{1}{\kappa/2 + i(\Delta + \Omega)} \right) E_{\text{cav}} e^{i\Omega t} - \right. \\ & \left. - \frac{\delta\varphi}{2} \left(1 - \frac{1}{\tau_{\text{ex}}} \frac{1}{\kappa/2 + i(\Delta - \Omega)} \right) E_{\text{cav}} e^{-i\Omega t} \right) + i \left(1 + \frac{\delta\varphi}{2} e^{i\Omega t} - \frac{\delta\varphi}{2} e^{-i\Omega t} \right) E_{\text{LO}}. \end{aligned} \quad (\text{S33})$$

If the laser is locked to line center, $\Delta \equiv 0$ and

$$|l|^2 = |l_{\text{DC}}^2 + \frac{1}{2} \cdot 2\text{Re} \left\{ \frac{\delta\varphi}{2} \left(1 - \frac{1}{\tau_{\text{ex}} \kappa/2 + i\Omega} \right) E_{\text{cav}} e^{i\Omega t} (-iE_{\text{LO}}) - \frac{\delta\varphi}{2} \left(1 - \frac{1}{\tau_{\text{ex}} \kappa/2 - i\Omega} \right) E_{\text{cav}} e^{-i\Omega t} (-iE_{\text{LO}}) + \left(1 - \frac{1}{\tau_{\text{ex}} \kappa} \right) E_{\text{cav}} \left(-i \frac{\delta\varphi}{2} e^{-i\Omega t} \right) - \left(1 - \frac{1}{\tau_{\text{ex}} \kappa} \right) E_{\text{cav}} \left(i \frac{\delta\varphi}{2} e^{i\Omega t} \right) \right\} = \quad (\text{S34})$$

$$= |l_{\text{DC}}^2 + \frac{1}{\tau_{\text{ex}}} \delta\varphi \Omega \sqrt{P_{\text{cav}} P_{\text{LO}}} \frac{2}{\kappa} \frac{(\kappa/2) \cos(\Omega t) + \Omega \sin(\Omega t)}{(\kappa/2)^2 + \Omega^2}, \quad (\text{S35})$$

such that the Hänsch-Couillaud signal resulting from this phase modulation is

$$h(t) = 2 \frac{\sqrt{P_{\text{LO}} P_{\text{cav}}}}{\tau_{\text{ex}}} \delta\varphi \Omega \frac{2}{\kappa} \frac{(\kappa/2) \cos(\Omega t) + \Omega \sin(\Omega t)}{(\kappa/2)^2 + \Omega^2}. \quad (\text{S36})$$

Comparison with the signal (S30) arising from harmonic displacement of amplitude x_0 , one can infer that phase modulation by $\delta\varphi$ leads to the same signal as a harmonic displacement of amplitude $x_0\omega_0/R\Omega$ —independent of cavity bandwidth, coupling conditions and readout power (note again that that sin- and cos-quadratures of the modulation add in quadrature). This can be used to calibrate the measured spectra by injecting a phase modulation of known depth at one particular frequency.

Experimentally, the modulation is produced using a fibre-coupled LiNbO₃-waveguide, to which a modulated voltage is applied. The depth of modulation for a certain applied voltage was derived by measuring the relative strengths of radio-frequency sidebands of a heterodyne beat of the modulated Nd:YAG laser with an independent diode laser at 1064 nm. A value of 17°/V was found, in good agreement with the specified value. We have checked that the residual amplitude modulation created in the modulator is negligible.

LASER NOISE HEATING

While the cooling laser, an external cavity grating-stabilized semiconductor laser, exhibits low intensity noise, its output was found to contain significant excess frequency noise even at the relevant Fourier frequencies above 10 MHz, as reported also by other groups [38]. Measurements against an independent cavity indicate frequency noise on the order of 200 Hz/ $\sqrt{\text{Hz}}$ for the Fourier frequencies of interest, corresponding to a phase noise of about 4 $\mu\text{rad}/\sqrt{\text{Hz}}$. To estimate the resulting heating effect it is first assumed the laser carries a sinusoidal phase modulation of depth $\delta\varphi$ at a Fourier frequency of Ω_m , the resonance frequency of the mechanical oscillator. Using the Bessel expansion for small $\delta\varphi$, the incoming light field can be written as

$$s_{\text{in}}(t) \cong \left(1 + \frac{\delta\varphi}{2} e^{+i\Omega_m t} - \frac{\delta\varphi}{2} e^{-i\Omega_m t} \right) s e^{i\omega t} \quad (\text{S37})$$

with the incoming amplitude s normalized such that $|s|^2 \equiv P$ is the optical power. Then the intracavity mode amplitude a (with $|a|^2$ normalized to intracavity energy) can be written as [35]

$$a(t) = \left(\frac{1}{\kappa/2 + i\Delta} + \frac{\delta\varphi e^{+i\Omega_m t}/2}{\kappa/2 + i(\Delta + \Omega_m)} - \frac{\delta\varphi e^{-i\Omega_m t}/2}{\kappa/2 + i(\Delta - \Omega_m)} \right) \frac{s e^{i\omega t}}{\sqrt{\tau_{\text{ex}}}}. \quad (\text{S38})$$

In the deeply resolved sideband regime $\kappa \ll \Omega_m$ this simplifies to

$$a(t) \cong \left(\frac{1}{-i\Omega_m} + \frac{\delta\varphi e^{+i\Omega_m t}/2}{\kappa/2} \right) \frac{s e^{i\omega t}}{\sqrt{\tau_{\text{ex}}}}. \quad (\text{S39})$$

if a detuning $\Delta = -\Omega_m$ is assumed. The intracavity energy therefore contains a modulation $\propto \sin(\Omega_m t)$ of amplitude $\delta\varphi/\Omega_m |s|^2$ for critical coupling $\tau_{\text{ex}} = 2/\kappa$. This gives rise to a modulated force of amplitude $\delta F = \delta\varphi P/\Omega_m R$, with R the cavity radius. Substituting $\delta\varphi$ with the measured phase noise *spectral density*, a noise force spectral density (SD) of

$$S_{F_{\text{noise}}} \cong \frac{S_\varphi P^2}{\Omega_m^2 R^2} \quad (\text{S40})$$

is obtained. This value can be considered constant for Fourier frequencies around Ω_m as long as $\Gamma_{\text{eff}} \ll \kappa$. An analogous approach yields a random force of spectral density $S_I P^2 / \Omega_m^2 R^2$ for a laser with a relative (i. e. normalized to I^2) intensity noise spectral density S_I . In the case of the employed laser we have measured that S_φ exceeds S_I by nearly four orders of magnitude, so that S_I can be neglected. Comparison with the thermal force SD $S_{\text{th}} = 2k_B T m_{\text{eff}} \Gamma$ then yields a power-dependent temperature of the laser

$$T_{\text{laser}} = \frac{1}{2k_B m_{\text{eff}} \Gamma} \frac{S_\varphi P^2}{\Omega_m^2 R^2} \quad (\text{S41})$$

Simultaneously, the laser cools the mode by modifying its susceptibility to the different noisy forces, with a rate $\Gamma_{\text{cool}} \cong \omega P / \Omega_m^3 m_{\text{eff}} R^2$ in the approximations described above. For a reservoir temperature T , the effective temperature of the mode is

$$T_{\text{eff}} \cong \frac{\Gamma}{\Gamma_{\text{cool}}} (T + T_{\text{laser}}). \quad (\text{S42})$$

The apparent contradiction of such a calculation with the properties of the *intensive* thermodynamical variable “temperature” is resolved by realizing that the quoted temperatures are effective temperatures representing uncorrelated random forces, which can be added in quadrature. For the optimum laser power of $P_{\text{opt}} = \sqrt{2k_B T m_{\text{eff}} \Gamma / S_\varphi} \cdot R \Omega_m$, the lowest achievable phonon occupancy is therefore found to be

$$n_{\text{min}} \cong \sqrt{2k_B T m_{\text{eff}} \Gamma S_\varphi} \frac{R \Omega_m}{\hbar \omega}. \quad (\text{S43})$$

With $T = 300$ K, $m_{\text{eff}} = 10$ ng, $\Gamma/2\pi = 1.3$ kHz, $\sqrt{S_\varphi} = 4$ $\mu\text{rad}/\sqrt{\text{Hz}}$, $k_B = 1.4 \cdot 10^{-23}$ J/K, $R = 38$ μm , $\Omega_m/2\pi = 40.6$ MHz, $\hbar = 1.05 \cdot 10^{-34}$ J s and $\omega/2\pi = 300$ THz, a minimum phonon number of about 5200 is found.
